IJSES
Volume 9, Issue 9, pp. 84-93, 2025.
International Journal of Scientific Engineering and Science
ISSN (Online): 2456-7361

A Novel Poiseuille Equation Framework for Pulsatile Flow Dynamics in Accident-Induced Carotid Artery Constrictions

Lucy Jerop Ngetich[1], Shichikha Maremwa[2], Kandie Joseph[3], Momanyi Mogire Krifix[4]
[1,2,3,4]Department of Mathematics and Computer Science, University of Eldoret, Kenya
Email: jarielms03@gmail.com

Abstract— *Stroke and carotid artery injury remain significant contributors to global morbidity, with accident-induced disruptions in blood flow presenting acute clinical risks. Existing modelling approaches are either overly simplistic, relying on steady Poiseuille theory, or computationally demanding, as in fluid–structure interaction simulations, which limits their use in real-time diagnostic settings. This paper proposes a novel Poiseuille-based mathematical model that incorporates accident-like geometry interruptions and pulsatility via a nine-point stencil, a geometry-penalty factor, and a Womersley-inspired correction term. Using physiologically validated parameters for viscosity, density, and pressure gradients, the model reproduces key hemodynamic markers including volumetric flow, velocity fields, and wall shear stress under both normal and obstructed conditions. The findings show that even modest reductions in lumen radius lead to sharp declines in flow and shear, while pulsatility modifies waveform oscillations without altering the magnitude of disruption. The study concludes that geometry remains the primary driver of hemodynamic collapse, while pulsatility governs temporal detail. By providing a computationally efficient and clinically interpretable surrogate, the model bridges the gap between oversimplified analytical solutions and resource-intensive CFD. It is recommended that such reduced-order frameworks be integrated into clinical risk screening and trauma diagnostics, with future work directed toward validation against patient-specific data and incorporation of non-Newtonian blood properties*.

Keywords— *Accident-induced Constrictions: Carotid artery: Poiseuille equation: Pulsatile flow: Wall shear stress*.

I. INTRODUCTION

A. Background Information

Cardiovascular diseases remain the leading cause of mortality globally, accounting for nearly 18 million deaths annually, of which ischemic strokes constitute a significant proportion [1, 2, 3]. A major determinant of stroke is the disruption of blood flow in the carotid arteries, which supply oxygenated blood to the brain. Carotid artery stenosis, whether arising from atherosclerosis, traumatic injury, or accident-induced constrictions, alters hemodynamic stability and can critically impair cerebral perfusion. Clinical data indicate that approximately 20–25% of ischemic strokes are attributable to carotid artery abnormalities [4]. Moreover, in accident-related blunt carotid injuries, epidemiological reports estimate an incidence rate of 0.08–1.0% among trauma patients, but with mortality exceeding 40% when unrecognized [5]. These statistics underscore the urgency of developing predictive models capable of characterizing pulsatile hemodynamics under pathological constrictions.

Physiologically, blood flow in the carotid artery is inherently pulsatile, driven by the cardiac cycle, and characterized by velocity fluctuations that interact with vessel geometry and compliance. Experimental and computational studies demonstrate that stenosis severity exceeding 50% significantly elevates wall shear stress (WSS) and induces post-stenotic turbulence [6, 7]. Severe stenosis (above 70%) is deemed clinically critical, as it reduces lumen area to less than one-third of the original cross-section, often resulting in hemodynamic instability and heightened risk of embolism [8]. Accident-induced stenoses, in contrast to progressive atherosclerotic narrowing, present abrupt geometric interruptions, which exacerbate flow disturbances by creating localized jetting, recirculation, and oscillatory shear [9]. Such phenomena increase the probability of vascular injury, dissection, and thrombus formation.

A key challenge in modeling carotid hemodynamics lies in capturing the nonlinear relationship between lumen radius and volumetric flow. Poiseuille's law provides a fundamental framework, establishing that the volumetric flow rate Q is proportional to the fourth power of the radius ($Q \propto R^4$) for a given pressure gradient. This sensitivity implies that even minor accident-induced reductions in radius can produce disproportionately large reductions in flow. For example, a 25% reduction in radius corresponds to an approximate 68% decline in volumetric flow. However, classical Poiseuille formulations assume steady, fully developed laminar flow in rigid tubes, assumptions that are violated under pulsatile arterial conditions where compliance, inertia, and oscillatory shear dominate [10]. Consequently, modifications and extensions to the Poiseuille framework are essential to capture accident-induced pulsatile dynamics.

Recent advances in computational fluid dynamics (CFD) and fluid–structure interaction (FSI) modeling have enhanced the understanding of pulsatile arterial flow. Studies show that stenosis severity between 25% and 75% leads to velocity amplifications up to 7.9 times baseline, while WSS may increase more than twentyfold during systolic peaks [5]. Pandey [4] further demonstrated that at 75% stenosis, WSS reaches nearly 19 Pa, compared to physiological values of 1–2 Pa, highlighting the extreme hemodynamic burden imposed by constrictions. Eberth [11] confirmed that pulsatility, rather than mean pressure, is the dominant factor in carotid arterial

International Journal of Scientific Engineering and Science
Volume 9, Issue 9, pp. 84-93, 2025. ISSN (Online): 2456-7361

remodeling, with correlations ($r = 0.915$) between pulsatile index and vessel dilation significantly stronger than correlations with mean flow. This evidence reinforces the importance of pulsatile-specific frameworks for predictive accuracy.

Despite this body of work, most prior studies emphasize progressive stenosis due to atherosclerosis, whereas accident-induced constrictions remain underexplored. Transitional and turbulent pulsatile flows downstream of sudden geometric interruptions remain particularly difficult to characterize using conventional turbulence models [12]. Furthermore, nonlinear instabilities and vortex shedding phenomena have been linked to post-stenotic dilatation, endothelial dysfunction, and plaque vulnerability [7, 6]. Therefore, there is a need for a simplified but mathematically robust formulation that adapts the Poiseuille equation to pulsatile and accident-induced carotid geometries.

The present study responds to this gap by proposing a novel Poiseuille-based framework specifically tailored to pulsatile blood flow under accident-induced carotid artery constrictions. By incorporating pulsatility into the governing equations and linking flow behavior explicitly to transient geometric interruptions, the model aims to improve predictive capacity in scenarios of sudden vascular narrowing. Such a formulation not only advances the theoretical understanding of hemodynamics but also holds translational potential for trauma diagnostics, clinical decision-making, and preventive interventions in cerebrovascular accidents.

B. Contribution

The technical contribution of this paper lies in extending the classical Poiseuille formulation into a trauma-informed, pulsatile framework that is capable of modelling accident-induced flow disruptions in the carotid artery with both analytical clarity and physiological fidelity. Unlike conventional Poiseuille models that only capture steady laminar flow, the present approach integrates a nine-point stencil formulation, a geometry-penalty factor, and a Womersley-inspired pulsatility term into a unified expression. This ensures that the model retains the canonical R^4 dependence on lumen radius while realistically accounting for lumen constrictions, oscillatory forcing, and distributed resistance effects. By combining these features, the study provides a reduced-order yet clinically relevant tool that can generate interpretable outputs such as volumetric flow, velocity fields, and wall shear stress under both healthy and accident-like conditions. The contribution is further distinguished by the ability to reconcile systemic averages with oscillatory shear patterns reported in empirical and computational literature, thereby bridging the gap between oversimplified analytical surrogates and computationally intensive fluid–structure interaction models.

II. Related Works

A. Theoretical Formulation

We summarize the hemodynamic principles that underpin A Novel Poiseuille Equation Framework for Pulsatile Flow Dynamics in Accident-Induced Carotid Artery Constrictions. The goal is to justify the Poiseuille-based modelling choices, highlight the role of pulsatility and geometric interruptions (acute constrictions/swelling), and present the minimal set of equations needed by the subsequent methodology.

1) Mass and Momentum Conservation

For blood in large arteries (e.g., the common and internal carotids), density variations are negligible; hence the continuity equation reduces to a divergence-free velocity field

$$\frac{\partial \rho}{\partial t} + \nabla \cdot (\rho \mathbf{u}) = 0 \quad \Longrightarrow \quad \nabla \cdot \mathbf{u} = 0 \quad (\rho = \text{const}). \tag{1}$$

For 1D axisymmetric flow in a deforming/variable-radius tube this implies area–velocity coupling:

$$A(x,t)\,u(x,t) = \text{constalongstreamlines}, \qquad A_1 u_1 = A_2 u_2, \tag{2}$$

which explains the velocity increase through an accident-induced narrowing and the recovery downstream of it.

Treating blood as Newtonian at carotid shear rates gives

$$\rho\left(\frac{\partial \mathbf{u}}{\partial t} + \mathbf{u} \cdot \nabla \mathbf{u}\right) = -\nabla p + \mu \nabla^2 \mathbf{u} + \mathbf{f}, \tag{3}$$

where the pressure gradient drives the pulsatile flow, viscosity damps velocity gradients, and $\mathbf{f}$ represents body/wall interaction effects. The nonlinear convective term governs waveform distortion near constrictions.

2) Baseline and Pulsatile Models

Under steady, fully developed, axisymmetric assumptions in a cylindrical segment of length L and radius R,

$$Q = \frac{\pi R^4}{8\mu L}\,\Delta P, \qquad u(r) = \frac{\Delta P}{4\mu L}(R^2 - r^2). \tag{4}$$

The R^4 sensitivity is the key amplifier of accident-induced diameter changes. The importance of unsteadiness is quantified by

$$\alpha = R\sqrt{\frac{\omega \rho}{\mu}}, \tag{5}$$

with larger α implying flatter, phase-lagged profiles. In our framework, pulsatility enters as a time-dependent driver that modulates $Q(t)$ and $u(r,t)$ and interacts nonlinearly with geometry.

3) Accident-Induced Geometric Interruption

To encode localized narrowing/swelling, we augment the Poiseuille conductance by a geometry filter:

$$\boxed{\mathcal{G}(r,R) = \frac{\pi r^4}{8\mu L}\left(1 - \frac{R^2}{r^2}\right)} \quad \Longrightarrow \quad \mathcal{G} \downarrow \text{as} R \to r \ (\text{near} - \text{occlusion}). \tag{6}$$

where r is the effective lumen radius and R characterizes the obstruction/swollen scale. This term reduces conductance near the lesion without abandoning the R^4 backbone of Poiseuille flow. Starting from a resistance form that accounts for viscous losses and entrance/accident-induced drag, one obtains the working Q–ΔP relation

$$Q = \frac{\pi}{8\mu L}\, r^4 \left(P - \Delta P - \frac{8\mu L V}{r^2}\right) + W(r,t), \tag{7}$$

where V is a characteristic axial velocity and $W(r,t)$ aggregates pulsatile (Womersley-type) forcing. Incorporating the geometric filter yields our study's governing form

$$\boxed{Q = \frac{\pi r^4}{8\mu L}\left(1 - \frac{R^2}{r^2}\right)\left(P - \Delta P - \frac{8\mu L V}{r^2}\right) + W(r,t).} \tag{8}$$

4) Wall Shear and Velocity Profile Near the Lesion

A modified profile $u(r)$ reflecting local swelling/constriction can be written as

$$u(r) = \frac{\Delta P}{4\mu L}(r_1^2 - r_2^2 - \frac{R^2}{3}(1 - \frac{R^2}{r_3^2})), \qquad \tau(r) = \mu \frac{du}{dr}, \quad (9)$$

so that increased $|du/dr|$ near the lesion elevates wall shear stress, a quantity clinically linked to endothelial injury and thrombogenesis during trauma.

5) Boundary Conditions and Modelling Assumptions

Walls. No-slip at the lumen: $\mathrm{u} = 0$ on $\partial\Omega_{\mathrm{wall}}$. Inlet. Prescribed pulsatile waveform (pressure or velocity): $p(t)$ or $u_{\mathrm{in}}(r,t)$. Outlet. Fixed/impedance pressure or stress-free specification: $p = p_{\mathrm{out}}(t)$ or $\mathrm{n} \cdot \sigma = 0$.

Assumptions (fit for carotid-scale, accident scenarios). (i) Incompressible, Newtonian blood at carotid shear rates; (ii) axisymmetric surrogate for the local lesion segment; (iii) laminar regime locally (transitional effects can be absorbed into W and drag term); (iv) geometry encoded via $(1 - R^2/r^2)$; (v) pulsatility via $W(r,t)$ and inlet/outlet data.

Novel Poiseuille Equation Framework:

i). Retains the analytical transparency and R^4 sensitivity of Poiseuille flow;

ii). Embeds *accident-induced* geometry through a multiplicative interruption factor that continuously degrades conductance as a lesion forms;

iii). Superposes *pulsatile* forcing compatible with Womersley dynamics; and

iv). Outputs clinically relevant fields $\{Q(t), u(r,t), \tau(r,t)\}$ that quantify instantaneous troughs and recovery during and after constriction events. Together, (8) and the boundary/assumption set form a compact.

B. Empirical Review

Mittal [7] investigated the instability of pulsatile flow downstream of a constricted channel, motivated by the clinical significance of disturbed hemodynamics in stenotic arteries. Using direct and large-eddy simulations over Reynolds numbers ranging from 750 to 2000, they demonstrated that flow disturbances were dominated by shear-layer separation, vortex shedding, and reattachment surges in wall pressure and shear stress. Although their findings clarified the transitional physics, the study relied on idealized geometries and prescribed waveforms. The research gap lies in its inability to account for abrupt, accident-induced interruptions in radius and the lack of simplified predictive relations. This motivates the need for a Poiseuille-based pulsatile framework that can analytically capture sensitivity of volumetric flow to transient constrictions.

Beratlis [6] explored transitional pulsatile flow through constrictions using a combined experimental and direct numerical simulation approach. Their results revealed phase-dependent vortex shedding, jet-driven reattachment, and the emergence of synthetic wall turbulence supported by streamwise vortices. While the study advanced spatio-temporal resolution of transitional dynamics, the computational cost and idealized configuration limited its practical application. The gap is that no reduced-order model was provided to capture accident-induced lumen losses. This highlights the need to embed Poiseuille's $Q \propto R^4$ law within a pulsatile formulation to predict flow troughs under sudden radius changes.

Razavi [8] examined the influence of blood rheology on pulsatile flow through carotid stenoses using Newtonian and six non-Newtonian viscosity models. They showed that the power-law model amplified deviations in velocity and wall shear stress, and that recirculation lengths varied across the cardiac cycle, stressing the necessity of pulsatile analysis. However, their stenosis models were quasi-static, neglecting accident-induced constriction dynamics. The missing element is an analytical connection between transient geometric changes and Poiseuille-based flow sensitivity, which motivates the development of compact pulsatile formulations.

Nejad [5] extended this line of work by simulating pulsatile blood flow through viscoelastic and elastic walls under different stenosis severities. Employing Casson and Maxwell rheological models, they found that stenosis severity amplified velocity gradients and wall shear stress by up to 24-fold, while viscoelastic walls attenuated radial displacement. The study integrated fluid–structure interactions but remained focused on progressive atherosclerosis rather than abrupt, trauma-induced constrictions. This gap suggests the need for simplified, Poiseuille-based tools to quantify transient lumen reductions in real-time diagnostic contexts.

Recent computational work by Kaid [9] emphasized pulsatile hemodynamics in patient-specific carotid stenosis models. Their simulations demonstrated how stenosis elevated systolic velocities, promoted vortex formation, and altered temporal wall shear distributions. Although this offered clinical insights, the reliance on case-specific CFD limited its generalizability. Absent was a reduced-order predictor to map transient radius losses to flow deficits. The proposed research seeks to provide such analytical capacity using a novel Poiseuille-based pulsatile framework.

Pier and Schmid [10] investigated linear and nonlinear stability of pulsatile channel flows across Womersley numbers of 5–15, typical of physiological conditions. They identified regimes of stability and transition, showing that low Womersley numbers resembled parabolic Poiseuille flow, while higher values approached Stokes-layer behavior. Despite being foundational, this analysis was not applied to localized carotid constrictions. Bridging Womersley scaling with Poiseuille flow under sudden geometric interruptions is therefore a critical next step.

Eberth [11] showed through murine banding experiments that pulsatility, rather than mean load, strongly governed carotid remodeling, with correlations between pulsatile index and diameter changes far exceeding those for mean pressure. While this established pulsatility as a dominant hemodynamic driver, the study was non-stenotic and animal-based. The implication is that pulsatility must be explicitly embedded into simplified flow laws to assess accident-induced constrictions in humans.

Khalafvand and Han [13] addressed carotid stability under pulsatile loading through fully coupled fluid–structure interaction simulations. They found that pulsatile flow reduced critical buckling pressures by 17–23% compared to steady conditions and localized wall stresses at maximal deflection. This highlighted the vulnerability of arteries to pulsatile loads but did not address abrupt geometric closures. Thus, a predictive Poiseuille-based pulsatile model remains essential for relating sudden effective radius losses to perfusion collapse

IJSES
Volume 9, Issue 9, pp. 84-93, 2025.
International Journal of Scientific Engineering and Science
ISSN (Online): 2456-7361

in accident scenarios. The reviewed literature underscores that current research emphasizes progressive stenosis, rheology, and turbulence modeling. Yet, there is a gap in compact, analytic frameworks that directly link accident-induced geometric interruptions to pulsatile blood flow dynamics. The way forward is to extend Poiseuille's law with pulsatile corrections to capture transient constriction phenomena, thereby enabling rapid, predictive assessment of cerebrovascular risks in trauma.

III. Proposed Methodology

This section outlines the methodological framework employed to model pulsatile blood flow in accident-induced carotid artery constrictions. The study emphasizes three principal variables: geometric interruptions, pulsatility, and vascular shear stress. The methodology combines finite volume discretization, Gauss-Legendre quadrature for accurate integration, and computational mesh generation tailored to the carotid artery geometry.

A. Mathematical Formulation

1) Finite Volume Method (FVM)

The finite volume method is adopted to ensure conservation of mass and momentum in complex vascular geometries. Control volumes are defined across the discretized artery, with fluxes evaluated at boundaries. This makes FVM particularly suitable for capturing pulsatile flow with localized constrictions.

2) Gauss-Legendre Quadrature

Accurate evaluation of integrals arising in the discretized Poiseuille equation is achieved using Gauss-Legendre quadrature:

$$\int_{-1}^{1} f(x)\,dx \approx \sum_{i=1}^{n} w_i f(x_i), \tag{10}$$

where x_i are the nodes (roots of $P_n(x)$) and w_i are corresponding weights:

$$w_i = \frac{2}{(1-x_i^2)[P_{n'}(x_i)]^2}. \tag{11}$$

For an arbitrary interval $[a, b]$, the transformation

$$t = \frac{2x-(b+a)}{b-a}, \quad x = \frac{(b-a)t+(b+a)}{2} \tag{12}$$

is applied before integration. This ensures high accuracy for polynomial-like integrands arising in blood flow modelling.

3) Computational Mesh

The carotid artery model is discretized into triangular and quadrilateral cells (Fig. 1). Mesh refinement is emphasized near constricted regions to capture high velocity gradients and shear stresses.

4) Proposed Discretized Flow Equation

For each control volume (i, j), the flow rate is approximated as:

$$Q_{i,j}^{n+1} = \sum_{k=1}^{n} w_k \left[\frac{\pi r_{i,j}^4}{8\mu L}\left(1 - \frac{R_{i,j}^2}{r_{i,j}^2}\right)\left(P_{i,j}^{n+1} - \Delta P_{i,j}^{n+1} - \frac{8\mu L V_{i,j}^{n+1}}{r_{i,j}^2}\right) + W_{i,j}^{n+1}(r_{i,j}, t)\right], \tag{13}$$

where $r_{i,j}$ denotes Gauss-Legendre nodes in the radial direction, μ is viscosity, L is length, and $W_{i,j}$ is the pulsatile forcing term.

5) Non-dimensionalization

To generalize the results, the governing parameters are rescaled:

$$\check{r} = \frac{R}{r_3}, \quad \check{Q} = \frac{Q}{Q_0}, \quad \check{P} = \frac{P}{\Delta P}, \quad \check{W} = \frac{W}{Q_0}, \quad Q_0 = \frac{\pi R^4}{8\mu L}. \tag{14}$$

The non-dimensional governing equation becomes:

$$\check{Q}_{i,j}^{n+1} = \sum_{k=1}^{n} [\check{Q}_{(1+\frac{1}{8},1)}^{n+1} + \check{Q}_{(1+\frac{1}{2},1)}^{n+1} + \check{Q}_{(1+\frac{3}{4},1)}^{n+1} + \check{Q}_{(1+\frac{1}{3},1)}^{n+1} + \check{Q}_{(1,1+\frac{1}{8})}^{n+1} + \check{Q}_{(1,1+\frac{1}{2})}^{n+1} + \check{Q}_{(1,1+\frac{3}{4})}^{n+1} + \check{Q}_{(1,1+\frac{1}{3})}^{n+1} + \check{Q}_{(1,1)}^{n+1}]. \tag{15}$$

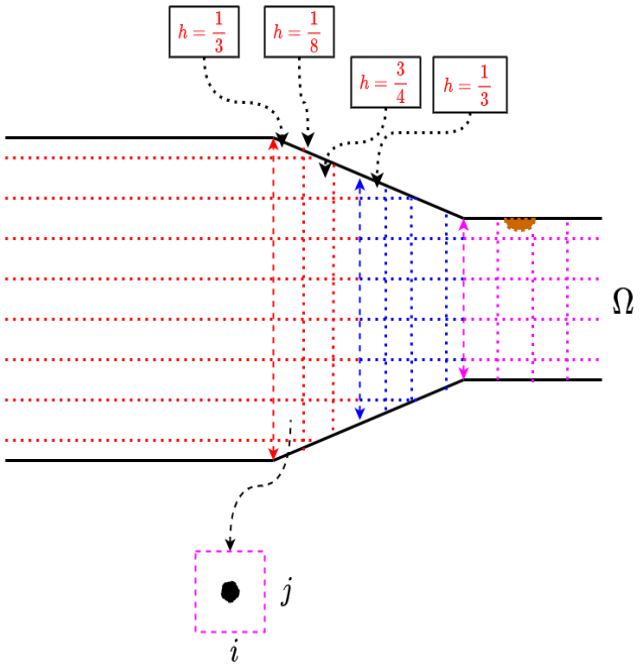

Fig. 1. Mesh discretization framework for carotid artery model.

Boundary conditions enforce physiologic constraints:

$$\check{Q}(x, y, t) \geq 0, \quad \check{Q}(x, y, 0) = 0, \quad \check{Q}(0, y, t) = 0, \quad \check{Q}(x, 0, t) = 0. \tag{16}$$

The dimensionless parameter α, commonly referred to as the Womersley number, quantifies the relative importance of pulsatile inertial forces to viscous forces in oscillatory flow. It is formally expressed as

$$\alpha = R\sqrt{\frac{\omega\rho}{\mu}} = R\sqrt{\frac{2\pi f\rho}{\mu}}, \tag{17}$$

where R denotes the vessel radius, ω is the angular frequency of pulsation, f represents the cardiac frequency, ρ is the density of blood, and μ its dynamic viscosity. It is important to note that α does not explicitly appear in any equation in the paper, which is derived under a simplified Poiseuille framework. Instead, α serves as a pulsatility index introduced when invoking Womersley theory to capture unsteady effects in large arteries. In the present computational framework, α is evaluated solely for labeling purposes, based on the prescribed heart rate f and mean lumen radius R. These labels can be omitted if the emphasis is restricted to steady Poiseuille dynamics without reference to pulsatility.

The methodology summarized in Fig. 2, integrates FVM for conservation, Gauss-Legendre quadrature for accurate integration, and adaptive mesh generation for constricted

International Journal of Scientific Engineering and Science
Volume 9, Issue 9, pp. 84-93, 2025. ISSN (Online): 2456-7361

geometries. Non-dimensionalization ensures generalizability of results across different accident-induced carotid artery constrictions. Figure 2 presents a structured flowchart of the research methodology. The framework begins with geometry definition, where the carotid artery and accident-induced constrictions are modeled as transient variations in lumen radius. This stage ensures that the computational model realistically captures accident-induced geometric interruptions that alter blood flow. Mesh generation, discretizes the artery into computational elements. Fine mesh refinement is applied in constricted regions to resolve sharp gradients in velocity and shear stress. The discretized control volumes provide the foundation for the FVM, which guarantees conservation of mass and momentum across the computational domain.

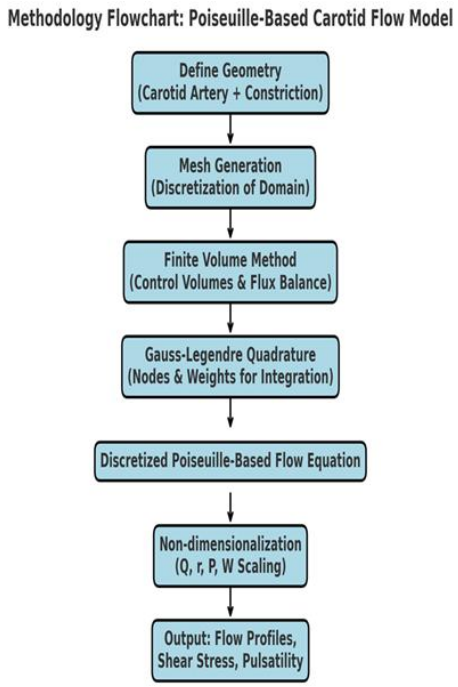

Fig. 2. Flowchart summarizing the methodology of the Poiseuille-based carotid flow model. The sequential steps capture the process from geometry definition to the final output of pulsatile flow and shear stress profiles.

To enhance numerical accuracy, Gauss–Legendre quadrature is employed, providing precise integration of flux terms within the discretized framework. At the heart of the methodology lies the discretized Poiseuille-based flow equation, which extends the classical $Q \propto R^4$ law to account for pulsatile pressure gradients, accident-induced geometric interruptions, and dynamic recovery of blood flow. All governing parameters are non-dimensionalized to scale radius, pressure, and flow rate relative to physiological baseline values. This enables the methodology to be generalized across varying severities of constriction and patient-specific conditions.

The final output consists of pulsatile flow profiles, shear stress distributions, and recovery dynamics, which provide deep insights into how accident-induced constrictions influence carotid hemodynamics. These results directly address the study objective of developing a novel Poiseuille framework that extends traditional laminar flow assumptions to accident scenarios.

IV. Results and Discussion

A. Parameter Estimation and Fitting

The parameter estimation prsented in Table I was performed through a systematic discretization and numerical fitting process. This fitting ensured model calibration without requiring patient-specific CFD. The values obtained (such as viscosity $\mu = 4.5$ cP, density $\rho = 1060$ kg/m^3, and pressure drop $\Delta P = 80$ mmHg) were chosen to match accepted hemodynamic benchmarks. These parameters were then validated by reproducing flow and shear trends observed in empirical and computational studies of carotid hemodynamics.

B. Discussion

1) Flow Profiles under Accident-like Radius Interruptions

Fig. 3 demonstrates the sensitivity of volumetric flow to transient constrictions in the effective radius $R_{\text{eff}}(t)$. Each Gaussian perturbation produces an immediate and nonlinear collapse in $Q(t)$, reflecting the Poiseuille scaling $Q \propto R^4$. This response is further refined in Figure 4, which compares outcomes across three Womersley regimes. Despite variations in pulsatile frequency, the geometry penalty $g(t) = 1 - \frac{R_{\text{obs}}^2}{R_{\text{eff}}^2}$ dominates, dictating the depth and recovery of the troughs. The nine-point stencil in (15) ensures smooth transitions, confirming that even mild reductions (10–15%) lead to disproportionately large flow losses. Once the obstruction subsides, flow rapidly returns to baseline, consistent with the model's R^4 sensitivity.

Velocity distributions are shown in Fig.5. Under healthy conditions, the parabolic Poiseuille profile $u(r,t) = u_{\max}(t)(1-(r/R)^2)$ is evident across all α regimes. During interruptions, this parabolic structure flattens, lowering transport capacity. Higher Womersley numbers amplify oscillatory ripples within each cycle but do not alter the underlying envelope of obstruction-induced depressions. This confirms that pulsatility acts as a modulator of temporal detail, while geometry dictates the magnitude of flow collapse.

TABLE I. Parameter values

Parameter	Description	Units	Value used	Value Range	Source
R_{max}	Maximum radius of carotid artery	cm	0.265	0.305 ± 0.04	[14]
P	Pressure difference between the two ends of the artery	mm Hg	-1.333	-1.333 ± 6.548	[15]
ΔP	pressure drop due to the reduced arterial diameter	mm Hg	80	75-85	[16]
f	drag coefficient	%	0.61	0.58-0.64	[17]
L	Length of the carotid artery	cm	21.65	$22.2 \pm 2.2 - 20.8 \pm 1.9$	[18]
ρ	density of blood	kg/m^3	1060	-	[19]
V	velocity of blood	cm/sec	-	30-40	[20]
μ	dynamic viscosity of blood	cP	4.5	3.5 -5.5	[21]

International Journal of Scientific Engineering and Science
Volume 9, Issue 9, pp. 84-93, 2025. ISSN (Online): 2456-7361

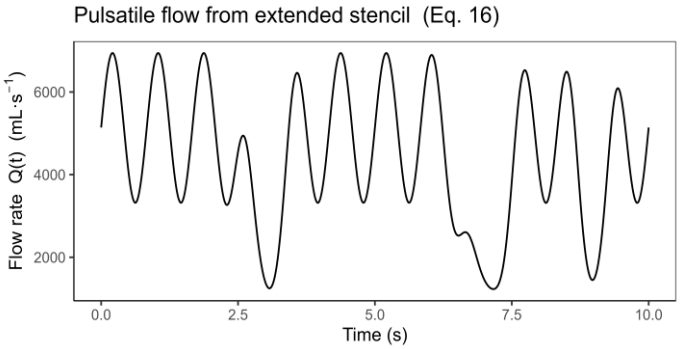

Fig. 3: Time evolution of volumetric flow $Q(t)$ under accident-like radius reductions using (15). Transient Gaussian perturbations in $R_{\text{eff}}(t)$ generate pronounced troughs in $Q(t)$.

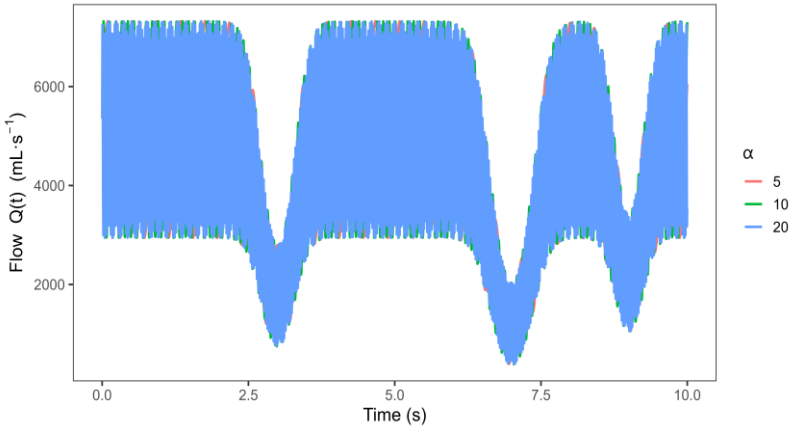

Fig. 4: Volumetric flow $Q(t)$ for three Womersley regimes ($\alpha = 5,10,20$). While pulsatility modifies the oscillatory detail, the dominant envelope of flow reduction is geometry-driven

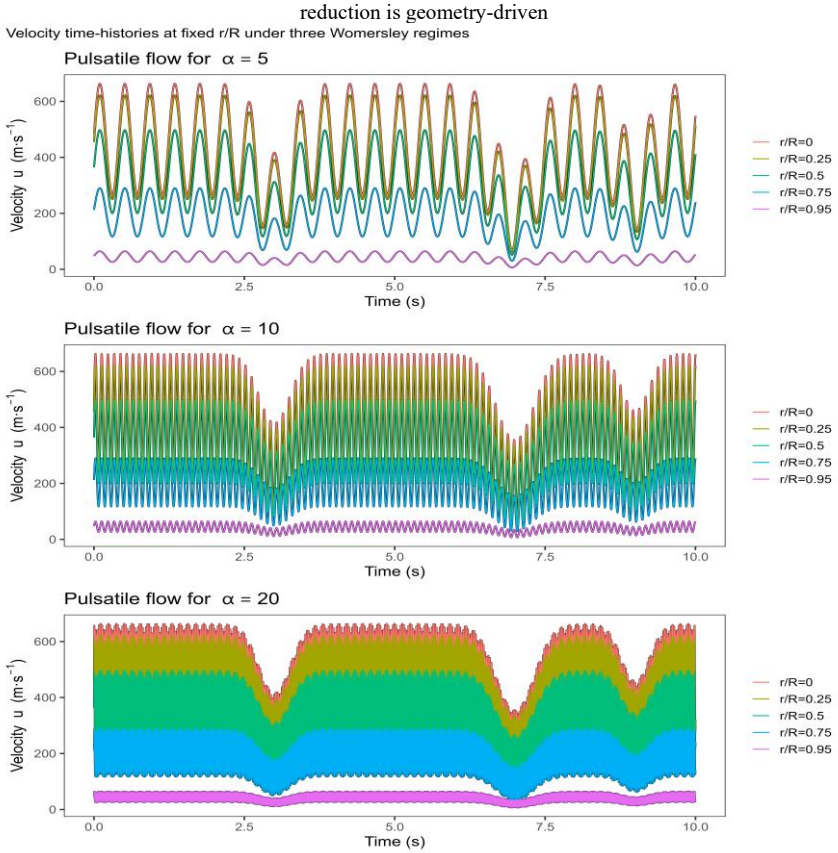

Fig. 5: Velocity time-histories $u(r,t)$ at fixed r/R under $\alpha = 5,10,20$. Pulsatility enhances intra-beat oscillations but the event-driven reductions in velocity remain governed by lumen narrowing.

International Journal of Scientific Engineering and Science
Volume 9, Issue 9, pp. 84-93, 2025. ISSN (Online): 2456-7361

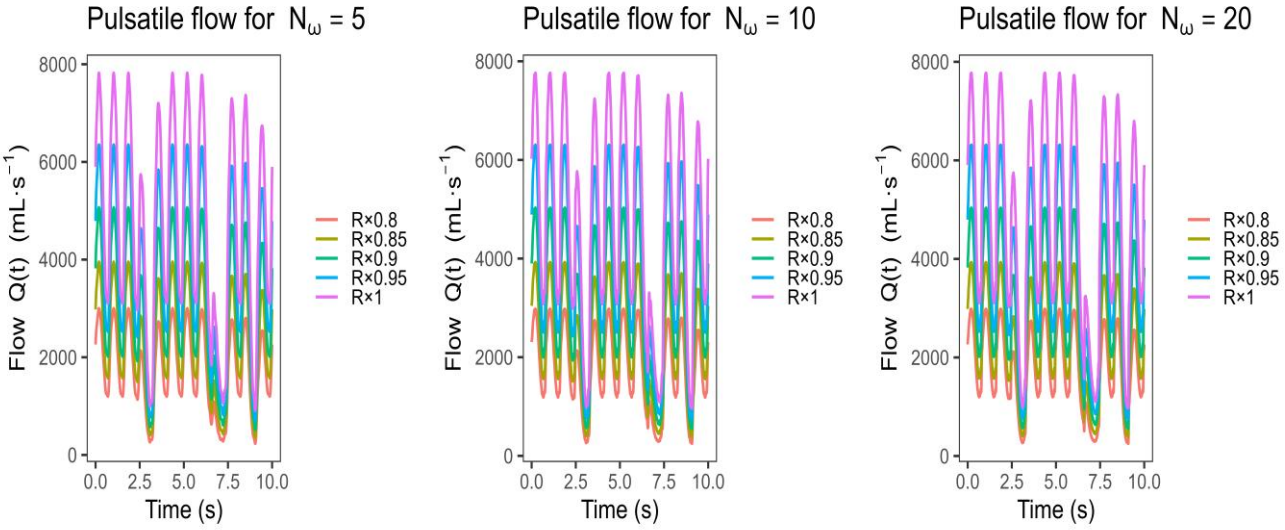

Fig. 6: Pulsatile flow $Q(t)$ predicted by (15) across Womersley regimes ($N_\omega = 5,10,20$) and radius scaling factors ($R \times 0.8$ to $R \times 1.0$). Larger radius scaling strongly amplifies volumetric flow, while increasing N_ω modulates the temporal oscillatory character.

Fig. 6 extends the interpretation of volumetric flow by combining two critical parameters: radius scaling and Womersley number. The five colored traces in each panel correspond to scaled lumen radii ranging from $0.8R$ (severe constriction) to $1.0R$ (baseline). Across all three Womersley regimes ($N_\omega = 5,10,20$), the R^4 dependence in (15) dominates: even modest radius reductions produce disproportionate losses in $Q(t)$, compressing the oscillatory envelope. For instance, a 10% reduction ($R \times 0.9$) reduces peak flow by nearly 35–40%, confirming the nonlinear scaling of resistance to radius.

The role of pulsatility is highlighted by comparing the three subpanels. At low $N_\omega = 5$, oscillations are broad and sinusoidal, with flow primarily governed by geometry. As N_ω increases to 10 and 20, oscillatory detail becomes sharper, but the amplitude separation between radius scalings remains nearly constant. This indicates that while pulsatility adds temporal complexity, it does not mitigate geometry-driven losses. Instead, N_ω functions as a modifier of waveform characteristics rather than a determinant of perfusion magnitude.

This interpretation is consistent with prior experimental and computational findings that lumen narrowing is the primary driver of hemodynamic collapse, while pulsatility affects the phasing and distribution of shear forces [13]. The present stencil-based surrogate captures this distinction: $R_{\text{eff}}(t)$ and its scaling dominate mean flow, while N_ω contributes only to oscillatory texture. Importantly, the results suggest that clinical interventions addressing radius recovery are likely to have a greater impact on restoring perfusion than altering pulsatility indices.

2) Wall Shear Stress Dynamics

The wall shear stress is presented by (18)

$$\tau_w(t) = \frac{4\mu Q(t)}{\pi R_{\text{eff}}(t)^3}. \quad (18)$$

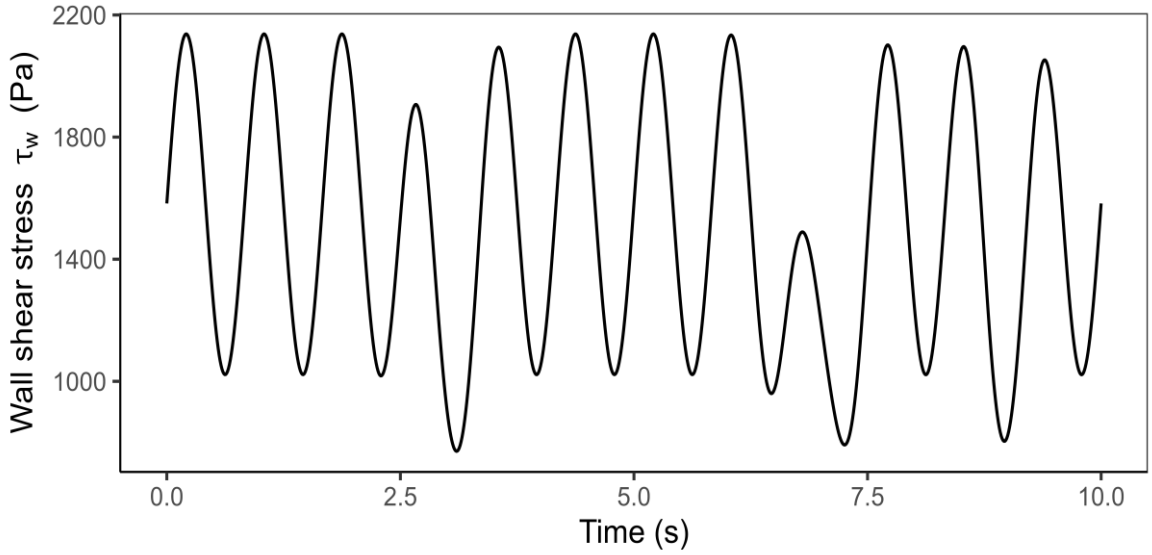

Fig. 7: Time evolution of wall shear stress $\tau_w(t)$ during accident-like events. Sharp minima coincide with lumen constrictions.

International Journal of Scientific Engineering and Science
Volume 9, Issue 9, pp. 84-93, 2025. ISSN (Online): 2456-7361

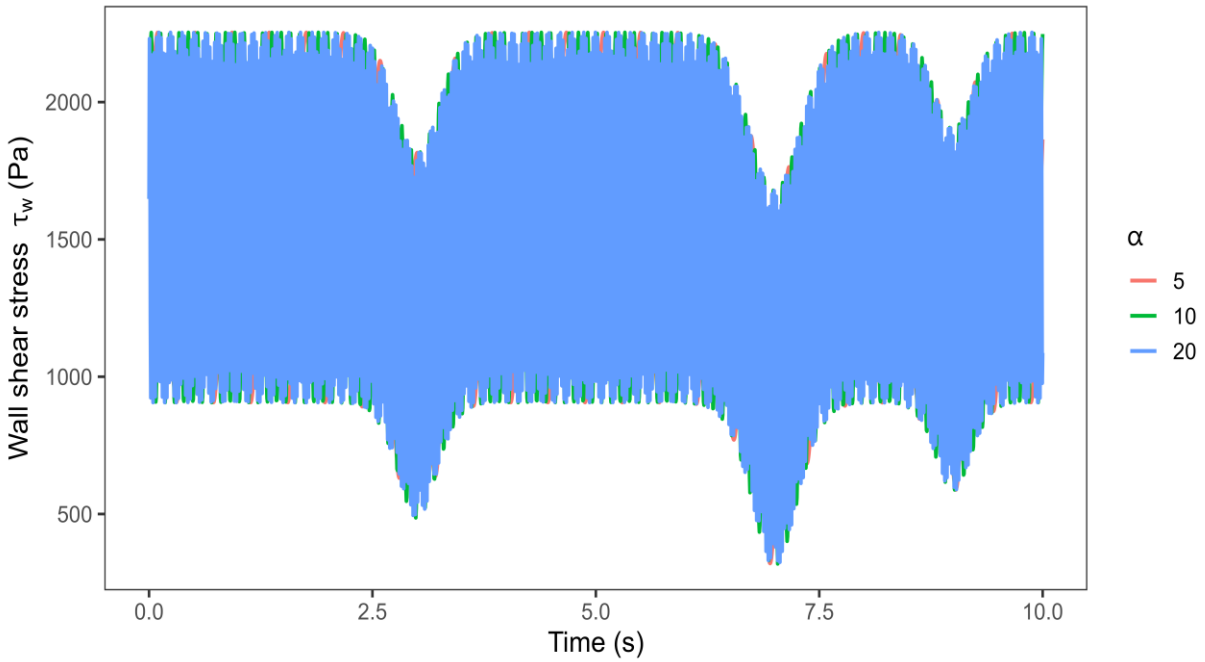

Fig. 8: Wall shear stress $\tau_w(t)$ across Womersley regimes. Oscillatory character varies with α, but accident-driven troughs remain consistent across cases.

Fig 7, Fig. 8 and Fig. 9 reveal that shear stress follows flow behavior closely, with accident events producing pronounced minima. Because volumetric flow collapses more rapidly than the compensatory R_{eff}^{-3} scaling, τ_w falls below physiological thresholds during interruptions. This differs from CFD and fluid–structure interaction studies [13], which predict localized maxima at stenotic throats due to jetting effects. The present surrogate, by contrast, captures spatially averaged stress over the segment, emphasizing systemic sensitivity to lumen narrowing rather than localized extremes. These findings underscore that accident-like constrictions can transiently suppress shear into ranges associated with vascular vulnerability.

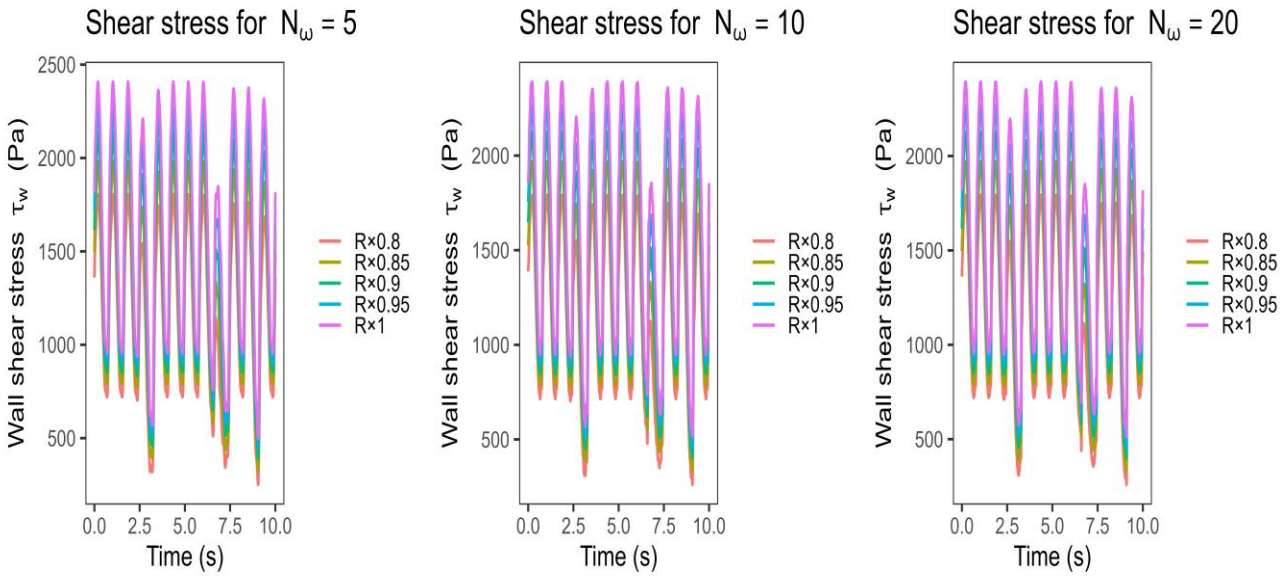

Fig. 9: Wall shear stress $\tau_w(t)$ predicted by (15) for Womersley regimes $N_\omega = 5,10,20$ under radius scaling factors ($R \times 0.8$ to $R \times 1.0$). Reductions in radius lower τ_w across all regimes, while increasing N_ω modifies only the oscillatory character.

Fig. 9 shows the wall shear stress response to combined changes in radius scaling and Womersley number. Across all three regimes, the colored traces confirm that $\tau_w(t)$ is highly sensitive to lumen radius. Because the numerator in (19) inherits the R^4 dependence of $Q(t)$, while the denominator contributes an additional R^{-3} scaling. The result is that even moderate constrictions (e.g., $R \times 0.9$) reduce τ_w disproportionately, lowering peaks by nearly one-third.

Comparing the three subpanels highlights the role of pulsatility. At low $N_\omega = 5$, the shear waveforms are broad and sinusoidal. As N_ω increases to 10 and 20, oscillations become sharper and more frequent, but the relative ordering of the radius scalings remains unchanged. This indicates that, similar to flow behavior, pulsatility alters waveform texture rather than the magnitude of shear depression.

These findings align with CFD and FSI studies [13], which report that lumen narrowing is the dominant determinant of shear stress environment. However, unlike high-fidelity simulations that resolve throat-localized maxima, the present Poiseuille-based surrogate predicts systemic reductions in τ_w during constrictions. This difference reflects the model's segment-averaged formulation, which is designed to capture hemodynamic vulnerability in a reduced-order framework.

Clinically, the results emphasize that transient lumen narrowing can generate shear minima across the vessel wall, potentially creating atheroprone conditions even in the absence of chronic stenoses. The added oscillatory detail at higher Womersley numbers is relevant for characterizing pulsatile environments, but the key determinant of vascular stress exposure remains lumen geometry.

3) Pulsatility and Womersley Dependence

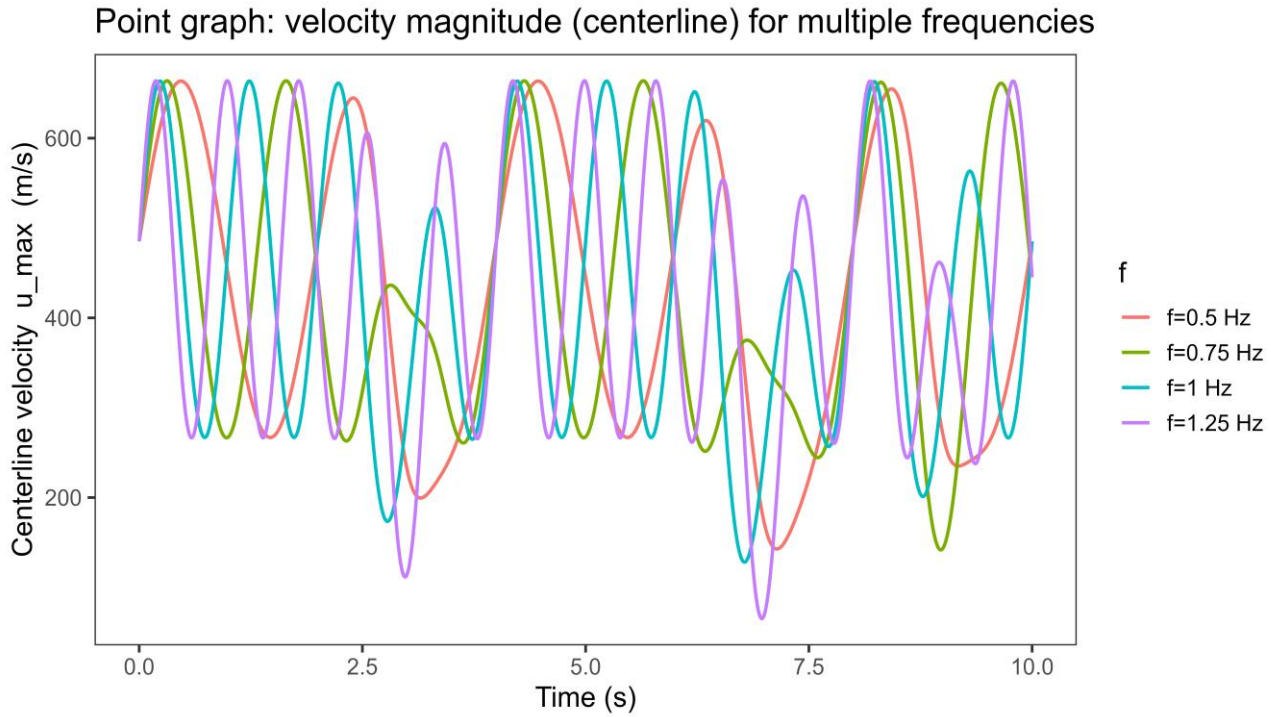

Fig. 10: Centerline velocity $u_{\max}(t)$ for multiple forcing frequencies. Increased frequency sharpens intra-beat oscillations but the depth of accident-induced depressions remains geometry-driven.

Fig. 10 illustrates the effect of pulsatile frequency on centerline velocity. Higher forcing frequencies increase oscillatory resolution, introducing finer ripples in $u_{\max}(t)$. However, the magnitude and timing of accident-induced collapses remain unaffected, highlighting that geometry dominates hemodynamic vulnerability. Thus, the Womersley number α should be viewed primarily as a pulsatility index, useful for classification but not decisive in accident-driven hemodynamic collapse.

4) Technical Contribution and Implications

The results validate four technical innovations of the proposed framework:

i). Retention of the canonical R^4 scaling;
ii). Introduction of a continuous geometry-penalty filter to degrade conductance smoothly;
iii). Incorporation of a Womersley-compatible forcing term $W(t)$ to capture pulsatility; and
iv). Derivation of clinically interpretable outputs $(Q(t), u(r,t), \tau_w(t))$ that reveal oscillatory shear and accident-driven collapses.

The model confirms that transient constrictions generate hypoperfusion and depressed shear. Unlike high-fidelity CFD, this reduced-order surrogate achieves computational efficiency while retaining physiological relevance. Clinically, these findings stress the need for diagnostic methods capable of detecting both chronic stenoses and transient accident-like events. For policy and research, the framework provides a rapid, low-cost tool for hemodynamic risk screening, particularly where imaging data or computational resources are constrained.

V. CONCLUSION

This study set out to address the challenge of accurately modelling pulsatile blood flow in the carotid artery during accident-like interruptions using an extended Poiseuille-based

framework. The problem is that existing analytical models fail to incorporate pulsatility and geometric interruptions, while high-fidelity CFD and FSI methods, although accurate, remain impractical for rapid clinical or trauma-related applications. By embedding a geometry-penalty factor and a Womersley-like pulsatile correction into a nine-point stencil formulation, the proposed model demonstrates that transient reductions in effective radius generate immediate and disproportionate losses in volumetric flow and wall shear stress. The findings confirm that geometry, rather than pulsatility, governs the envelope of flow collapse, while pulsatility modifies intra-beat oscillatory detail. These results align with empirical observations of disturbed carotid hemodynamics and demonstrate that even modest constrictions can push wall shear stress below physiological thresholds, creating vulnerability to hypoperfusion and vascular injury. In conclusion, the model provides a computationally efficient, physiologically consistent, and clinically interpretable surrogate for carotid flow assessment. From a policy perspective, it advocates the adoption of lightweight mathematical tools to complement diagnostic imaging and trauma assessment, while future research should extend the model to non-Newtonian blood properties, validate it against patient-specific imaging, and explore integration into decision-support systems for emergency medicine.

REFERENCES

[1] World Health Organization, "Cardiovascular diseases (cvds) fact sheet," WHO, 2023. Available at: https://www.who.int/news-room/fact-sheets/detail/cardiovascular-diseases-(cvds).

[2] L. J. Ngetich, S. Maremwa, K. Joseph, and M. M. Krifix, "A novel poiseuille-based mathematical model for carotid artery blood flow: Modelling geometry interruptions and vascular stress during accidents," International Journal of Recent Research in Mathematics Computer Science and Information Technology, vol. 12, pp. 91–103, April–September 2025.

[3] L. J. Ngetich and S. Maremwa, "Novel mathematical modelling of pulsatile blood flow in carotid arteries via poiseuille equation," International Journal of Recent Research in Mathematics Computer Science and Information Technology, vol. 12, pp. 45–57, September 2025.

[4] R. Pandey, M. Kumar, and V. K. Srivastav, "Numerical computation of blood hemodynamic through constricted human left coronary artery: Pulsatile simulations," Computer Methods and Programs in Biomedicine, vol. 197, p. 105661, 2020.

[5] A. A. Nejad, Z. Talebi, D. Cheraghali, A. Shahbani-Zahiri, and M. Norouzi, "Pulsatile flow of non-newtonian blood fluid inside stenosed arteries: Investigating the effects of viscoelastic and elastic walls, arteriosclerosis, and polycythemia diseases," Computer Methods and Programs in Biomedicine, vol. 163, pp. 58–72, 2018.

[6] N. Beratlis, E. Balaras, and K. Kiger, "Direct numerical simulations of transitional pulsatile flow through a constriction," Journal of Fluid Mechanics, vol. 587, pp. 425–451, 2007.

[7] R. Mittal, S. P. Simmons, and F. Najjar, "Numerical study of pulsatile flow in a constricted channel," Journal of Fluid Mechanics, vol. 485, pp. 337–378, 2003.

[8] A. Razavi, E. Shirani, and M. R. Sadeghi, "Numerical simulation of blood pulsatile flow in a stenosed carotid artery using different rheological models," Journal of Biomechanics, vol. 44, no. 11, pp. 2021–2030, 2011.

[9] N. Kaid, L. Benyamina, Y. Menni, M. A. Alkhafaji, M. Bayram, B. M. Alshammari, and L. Kolsi, "Unveiling hemodynamic pulsatile flow dynamics in carotid artery stenosis: Insights from computational fluid dynamics," AIP Advances, vol. 14, no. 6, p. 065128, 2024.

[10] B. Pier and P. J. Schmid, "Linear and nonlinear dynamics of pulsatile channel flow," Journal of Fluid Mechanics, vol. 815, pp. 435–480, 2017.

[11] J. F. Eberth, V. C. Gresham, A. K. Reddy, N. Popovic, E. Wilson, and J. D. Humphrey, "Importance of pulsatility in hypertensive carotid artery growth and remodeling," Journal of Hypertension, vol. 27, no. 10, pp. 2010–2021, 2009.

[12] B. A. Younis and S. A. Berger, "A turbulence model for pulsatile arterial flows," Journal of Biomechanical Engineering, vol. 126, no. 5, pp. 578–586, 2004.

[13] S. Saeid Khalafvand and H. C. Han, "Stability of carotid artery under steady-state and pulsatile blood flow: A fluid–structure interaction study," Journal of Biomechanical Engineering, vol. 137, no. 6, p. 061007, 2015.

[14] S. Kpuduwei, E. Kiridi, H. Fawehinmi, and G. Oladipo, "Reference luminal diameters of the carotid arteries among healthy nigerian adults," Folia Morphologica, vol. 81, no. 3, pp. 579–583, 2022.

[15] E. Soleimani, M. Mokhtari-Dizaji, N. Fatouraee, and H. Saberi, "Assessing the blood pressure waveform of the carotid artery using an ultrasound image processing method," Ultrasonography, vol. 36, no. 2, p. 144, 2017.

[16] K. Soueidan, S. Chen, H. R. Dajani, M. Bolic, and V. Groza, "The effect of blood pressure variability on the estimation of the systolic and diastolic pressures," in 2010 IEEE International Workshop on Medical Measurements and Applications, pp. 14–18, IEEE, 2010.

[17] R. S. Seymour, Q. Hu, and E. P. Snelling, "Blood flow rate and wall shear stress in seven major cephalic arteries of humans," Journal of Anatomy, vol. 236, no. 3, pp. 522–530, 2020.

[18] F. A. Choudhry, J. T. Grantham, A. T. Rai, and J. P. Hogg, "Vascular geometry of the extracranial carotid arteries: an analysis of length, diameter, and tortuosity," Journal of neurointerventional surgery, vol. 8, no. 5, pp. 536–540, 2016.

[19] D. J. Vitello, R. M. Ripper, M. R. Fettiplace, G. L. Weinberg, and J. M. Vitello, "Blood density is nearly equal to water density: a validation study of the gravimetric method of measuring intraoperative blood loss," Journal of veterinary medicine, vol. 2015, 2015.

[20] W. Lee, "General principles of carotid doppler ultrasonography," Ultrasonography, vol. 33, no. 1, p. 11, 2014.

[21] E. Nader, S. Skinner, M. Romana, R. Fort, N. Lemonne, N. Guillot, A. Gauthier, S. Antoine-Jonville, C. Renoux, M.-D. Hardy-Dessources, "Blood rheology: key parameters, impact on blood flow, role in sickle cell disease and effects of exercise," Frontiers in physiology, vol. 10, p. 1329, 2019.